nature climate change

LETTERS

PUBLISHED ONLINE: 4 MARCH 2012 | DOI: 10.1038/NCLIMATE1433

Black-carbon reduction of snow albedo

Odelle L. Hadley* and Thomas W. Kirchstetter

Climate models indicate that the reduction of surface albedo caused by black-carbon contamination of snow contributes to global warming and near-worldwide melting of ice[1,2]. In this study, we generated and characterized pure and black-carbon-laden snow in the laboratory and verified that black-carbon contamination appreciably reduces snow albedo at levels that have been found in natural settings[1,3,4]. Increasing the size of snow grains in our experiments decreased snow albedo and amplified the radiative perturbation of black carbon, which justifies the aging-related positive feedbacks that are included in climate models. Moreover, our data provide an extensive verification of the snow, ice and aerosol radiation model[1], which will be included in the next assessment of the Intergovernmental Panel on Climate Change[5].

Snow is among the most reflective of natural surfaces on Earth. Addition of dark impurities decreases its reflectance, also known as albedo, and increases its absorption of solar energy. In 1950s Soviet Central Asia, following a practice dating back to the time of Alexander the Great, snow was intentionally darkened with coal dust to accelerate glacial melting and increase the supply of irrigation water. In contrast, present-day, impurity-enhanced glacial melting that stems from the pollution of snow with trace amounts of black carbon (BC) is unintended and a cause for concern[1,2,6].

BC, a main component of microscopic soot particles produced from the burning of diesel, coal and biomass, strongly absorbs solar radiation. Radiation-transfer calculations indicate that seemingly small amounts of BC in snow, of the order of 10–100 parts per billion by mass (ppb), decrease its albedo by 1–5% (refs 2,7,8). When included in climate models, this BC-induced albedo reduction constitutes a positive radiative climate forcing that contributes to global and regional warming because less solar energy is reflected back to space. The globally averaged radiative forcing from BC contamination of snow is small (0.05 W m^{-2}), but regional forcing over snow-covered regions, such as the Arctic and the Himalayas (0.6 and 3.0 W m^{-2}, respectively), are comparable to the perturbation caused by the accumulation of carbon dioxide in the atmosphere since preindustrial times (1.5 W m^{-2}; ref. 1).

Although it may seem surprising that trace amounts of BC in snow can have significant climate effects, there are several, not immediately obvious, contributing factors at play. Compared with other constituents of atmospheric particulate matter that deposit in snow, notably dust, BC absorbs solar radiation most efficiently[2]. The absorbing efficiency of BC is higher in snow than in the atmosphere because sunlight is scattered more in snow than in air, which increases the probability of interaction with BC (ref. 9). Additionally, the BC–snow forcing is more impactful than indicated by a direct comparison with the CO_2 forcing because, according to climate models[1,2], BC warms the planet two to three times more than CO_2 for the same instantaneous W m^{-2} of forcing[1].

The greater warming, or efficacy, of the BC–snow forcing is the result of positive feedbacks, including a BC-caused acceleration in the growth of snow grains that further decreases albedo[1]. Snow grains naturally grow as they age, and larger grains allow sunlight to travel deeper into a snowpack, which reduces the surface albedo[10–12]. A positive feedback is included in climate models because the absorption of sunlight by BC in snow is expected to cause the grains to melt, fuse and grow faster than would occur in pure snow. Also, models of radiation transfer in snow predict that a fixed amount of BC will reduce the surface albedo of larger-grained snow more than it would in snow with smaller grains[1,8,11,13,14].

Radiation-transfer models of pure-snow albedo have been validated by measurements[14–16] and a recent study found good agreement between theory and measured albedo reduction owing to 2,500 ppb BC in snow[13]. However, model predictions of BC-caused snow-albedo reduction over a range of BC levels and snow grain sizes have not been verified by measurements. The main reason is that the BC effect is typically masked in natural environments by other variables that influence albedo, such as snow grain size, snow density, snow depth and the interaction of sunlight with the underlying surface, tree cover and solar zenith angle[7,13,17]. Consequently, measurements of artificial homogeneous snow with high concentrations of BC are needed. Experiments of this nature are being conducted both outdoors[13] and, as we have done here, in the laboratory.

Here, we developed a new approach to isolate the effect of BC on snow albedo through laboratory experimentation. We developed processes for making both pristine and BC-laden snow and techniques for measuring the morphology, albedo and BC content of snow. These methods have allowed us to quantify the snow-albedo reduction associated with increasing amounts of BC and as a function of snow grain size. With the most extensive data set available so far, we compared our experimental observations with the output of the snow, ice and aerosol radiation (SNICAR) model as a step towards verifying or refuting the predicted climate impacts of BC in snow.

We made snow in the laboratory with BC concentrations ranging from 0 to 1,700 ppb, which spans the range of BC concentrations measured in snow worldwide[1,3,18,19]. Laboratory snow grains were spherical, equivalent to those of snowpacks simulated by models[1,16] and resembling naturally aged snow grains that have been rounded by forces of temperature and pressure[10] better than freshly fallen flakes. We examined different sizes of snow grains characterized by optical effective radii (R_{eff}) of 55, 65 and 110 μm.

The spectral albedo of snow measured in our experiments and simulated with the SNICAR model is shown in Fig. 1. We ran the model with a solar zenith angle of 0° to be consistent with our experimental method of measuring albedo and with BC concentrations and effective snow grain sizes that matched our experimental values. SNICAR is described in Supplementary Section S7. Model parameters simulated an infinitely deep snowpack, eliminating the influence of the underlying surface on albedo. Our measurements have been scaled by the amounts shown in Supplementary Fig. S5 (<1% adjustment in most cases) so that they are representative of an infinite snow depth (Supplementary Section S6).

Lawrence Berkeley National Laboratory, 1 Cyclotron Road, Berkeley California 94720, USA. *e-mail: olhadley@lbl.gov.

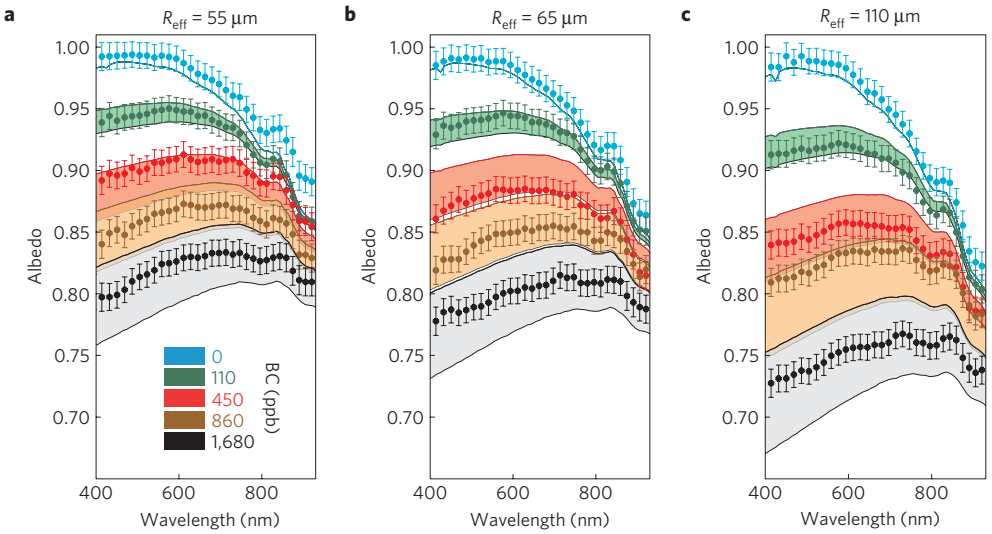

Figure 1 | Spectral albedo of snow of different R_{eff} measured in our experiments (dots) and modelled using SNICAR (shaded bands). a, 55 μm R_{eff}, **b**, 65 μm R_{eff} and **c**, 110 μm R_{eff}. Error bars show the standard deviation of the measurements. Upper and lower boundaries of the shaded bands correspond to modelled albedo assuming BC mass absorption cross-sections, at $\lambda = 550$ nm, of 7.5 and 15 $m^2\ g^{-1}$, respectively.

The spectral albedos of pure snow derived from our measurements and simulated with SNICAR are in good agreement. More notably, we measured decreasing snow albedo with increasing levels of BC contamination, confirming the fundamental premise of a BC-induced snow-albedo reduction. The convergence of spectral albedo at wavelengths greater than 700 nm, for pure and BC-contaminated snow samples alike, shows that the radiative perturbation of BC is largest in the visible and becomes insignificant in the near-infrared region of the solar spectrum, as previously hypothesized[8]. The reason is that ice strongly absorbs infrared radiation and masks the BC absorption, which decreases with increasing wavelength[8].

The wide span in the simulated spectral albedo of BC-contaminated snow (Fig. 1, shaded regions) illustrates sensitivity to the mass absorption cross-section (MAC) of BC—a measure of how much sunlight BC particles can absorb. Referring to natural variation in BC MAC by as much as a factor of two, Bohren previously asserted that predicting snow albedo requires more information about BC than is readily obtainable[20]. Today, however, improved instrumentation more readily provides measurements of BC MAC. The upper limit of simulated spectral albedo in Fig. 1 corresponds to a BC MAC equal to 7.5 $m^2\ g^{-1}$ (at 550 nm), the value assumed in a recent climate assessment[1] and an appropriate value for freshly emitted BC (ref. 21). The lower limit corresponds to snow contaminated with BC that is twice as absorbing (MAC = 15 $m^2\ g^{-1}$), which matched the BC in our experiments (Supplementary Section S3) and is an appropriate value for atmospherically aged BC (ref. 22).

Based on our spectral albedo measurements and the properties of ice in the near infrared, we estimated the spectrally weighted albedo of snow over the 300–2,500 nm solar spectrum. As shown in Fig. 2, the albedo of both pure and BC-contaminated snow is lower when snow grains are larger. For example, measurements and model alike show that increasing R_{eff} from 55 to 110 μm decreases pure-snow albedo by 0.05 (from 0.82 to 0.77), increasing solar absorption in snow by 28%. In Fig. 3, we show for each snow grain size the albedo reduction attributable only to BC ($\Delta\alpha_{BC}$), calculated as the difference between pure- and BC-contaminated snow albedo. These data reveal an effect that is not obvious in Figs 1 and 2: the radiative perturbation of BC in snow is amplified with increasing snow grain size, as Warren and Wiscombe predicted[23]. For example, the albedo reduction attributable to 300 ppb of BC is 20% larger

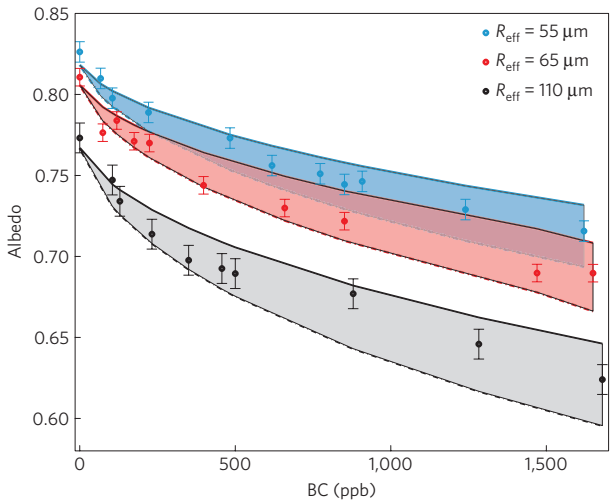

Figure 2 | Spectrally weighted snow albedo over the 300–2,500 nm solar spectrum: derived from our experiments (dots, ±1 standard deviation) and modelled using SNICAR (shaded bands). Upper and lower boundaries of the shaded bands correspond to modelled albedo assuming BC mass absorption cross-sections, at $\lambda = 550$ nm, of 7.5 and 15 $m^2\ g^{-1}$, respectively.

in 110 μm snow (−0.06) than it is in 55 μm snow (−0.05). Thus, our measurements support the inclusion of a positive feedback in climate models to account for the increased solar energy absorbed by BC in ageing snow.

To illustrate the combined influences of grain growth and BC contamination on snow-albedo reduction, we can express the overall albedo change as the sum of three components: the albedo change (−0.05) that occurs when pure snow grows from 55 to 110 μm, that owing to the 300 ppb BC contamination of initially 55 μm snow (−0.05), and the incremental change in albedo (−0.06+0.05 = −0.01) owing to the amplification of BC's radiative perturbation when the snow grows to 110 μm. Thus, compared with pure 55 μm snow, 300 ppb BC contamination and growth to 110 μm causes a net albedo reduction of 0.11 (from 0.82 to 0.71), causing the snow to absorb 61% more solar energy. In this example, a little more than half of the additional energy absorbed would be owing to BC.

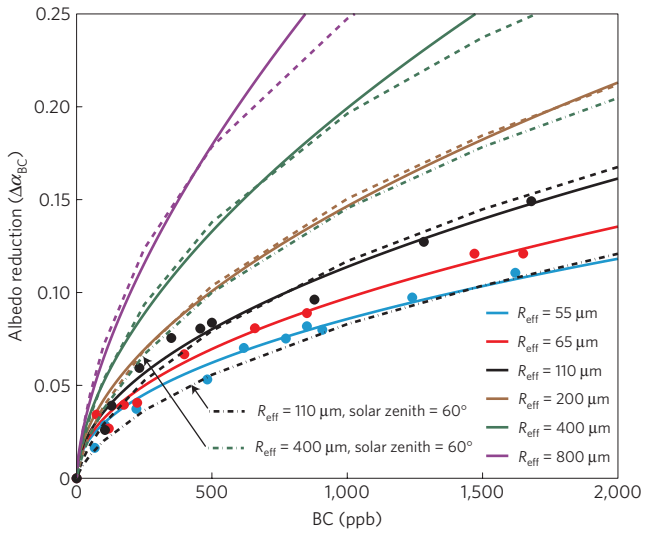

Figure 3 | Snow-albedo reduction attributed to BC computed as the albedo of pure snow minus the albedo of BC-contaminated snow for a 0° solar zenith angle (unless otherwise noted). Filled circles show experimental data for snow with R_{eff} of 55, 65 and 110 μm. Solid lines are the result of an empirical model derived from our data and predict BC's radiative perturbation in larger-grained snow. The dashed lines show SNICAR predictions for a BC MAC of 11 m^2 g^{-1} at 550 nm. The dash-dot lines show SNICAR predicted albedo reduction at two R_{eff} for a 60° solar zenith angle.

To estimate the albedo reduction owing to BC in snow with grains larger than we could measure in our experiments, we derived an empirical model from a least-squares fit of our data: $\Delta\alpha_{BC} = 0.0035\,BC^k$, where $k = 0.295\,(R_{eff}^{0.114})$ and BC concentration and snow-grain R_{eff} are expressed in units of ppb and μm, respectively. Empirically determined $\Delta\alpha_{BC}$ is plotted in Fig. 3 (solid lines) for R_{eff} of 110, 200, 400 and 800 μm, sizes that are typical of snow in spring[17,24]. Our model predicts that the radiative perturbation of BC in snow continues to increase as snow grains grow: the BC-caused snow-albedo reduction and, thus, the energy absorbed by snow increases by nearly 50% for each doubling of R_{eff}.

Both measurements and simulations show that snow albedo is most sensitive to BC (that is, snow-albedo decrease is steepest with increasing BC) at concentrations below 200 ppb. For example, 200 ppb is required to decrease the albedo of 110 μm R_{eff} snow by 5%, whereas only 10–20 ppb of BC, a concentration level that is typical for many natural environments[1], decreases snow albedo by 1% (Fig. 3). A 1% albedo decrease, as noted above, is expected to contribute to global warming and accelerate ice melting[1,2].

It is important to note that, by virtue of our method of albedo measurement, our results strictly apply to a solar zenith angle of 0°. This mimics sunlight striking normal to the snow surface and yields the strongest albedo response to the BC contamination[16]. Thus, whereas our results demonstrate a BC-caused snow-albedo reduction and confirm previously modelled effects, the climate implications of BC in snow are more appropriately inferred from a more climatically relevant solar zenith angle of 60°. With the sun lower in the sky, predicted albedo reductions owing to BC are lower, as shown in Fig. 3 (dash–dot lines) for snow-grain R_{eff} of 110 and 400 μm.

Our measured and extrapolated $\Delta\alpha_{BC}$ compare best to the SNICAR model (dashed lines in Fig. 3) for all snow grain sizes when we prescribed BC MAC = 11 m^2 g^{-1}, a value corresponding to the middle of the shaded regions in Figs 1 and 2. When run with MAC = 15 m^2 g^{-1} (not shown), SNICAR predicted much larger amplification in the BC-caused albedo reduction than our empirical model predicted for the larger-R_{eff} snow. Although our experiments provide an extensive verification of simulated snow-albedo reduction owing to BC (Figs 1–3), some uncertainty remains about BC-induced albedo reduction that could be addressed by additional experiments with larger-grained snow.

Last, we note that potential increase in the rates of melting and grain growth owing to the extra solar energy absorbed in BC-contaminated snow—which contributes to the high warming efficacy—also merits experimental study. Although we did not measure melt rate, our data are consistent with one study that measured enhanced snow-melt rate in BC-contaminated snow relative to a pure snowpack. Conway *et al.*[17] measured a snow-albedo reduction of 0.21 and a 50% increase in the ablation rate of natural snow attributed to 500 ppb BC contamination. Our empirical model predicts that 500 ppb BC would reduce pure-snow albedo by 0.21 if R_{eff} was 1, 150 μm, which is reasonably close to the effective radius of 1,000 μm estimated by Conway and colleagues.

Methods

In the laboratory, we made snow by freezing droplets of water sprayed into a 1.3-m-tall Styrofoam-insulated chamber cooled to −100 °C with liquid nitrogen. Pristine and BC-containing snow were made by spraying pure water and aqueous suspensions of BC, respectively. Aqueous BC suspensions were made using gravimetrically measured amounts of flame-generated BC (ref. 25) turned hydrophilic through exposure to ozone[26,27] (Supplementary Section S1). BC concentrations in melted snow samples were measured by absorption spectroscopy with ppb-level sensitivity using a liquid waveguide capillary cell (Supplementary Section S2). We controlled the size of the snow grains by varying the pressures applied to different spray nozzles.

Using a digital microscope (Dino-Lite Pro, model AM413TS) at magnification ×500 revealed that our laboratory snow grains were spherical (Supplementary Fig. S3). Snow-grain effective radius—a single radius that would yield the same albedo if the snow grains were monodisperse rather than polydisperse in size—was determined from spectral snow albedo between 1,000 and 2,500 nm (Supplementary Fig. S4). Spectral snow albedo in this infrared region is highly sensitive to and commonly used to estimate snow grain size[13,15,24].

Snow albedo was measured using a spectrometer equipped with an integrating sphere (15 cm in diameter) by normalizing the reflectance of snow samples to that of a NIST-certified standard whose reflectance was Lambertian and ranged from 0.987 to 0.985 throughout the visible portion of the solar spectrum. A Lambertian surface scatters radiation in all directions according to a cosine function and snow is approximately Lambertian. Here, we measured snow albedo from 395 to 950 nm, the region of the solar spectrum where the radiative perturbation of BC contamination is largest[1,2,8].

It has been shown that use of an integrating sphere-equipped spectrometer yields the same spectral reflectance and, when integrated over the solar spectrum, the same albedo as a pyranometer system[28], which is the common system for measuring solar reflectance of large surfaces, such as a field of snow with a length scale of several metres[13,17]. We discuss a key challenge of the sphere/spectrometer method below and our approach to minimizing measurement error. Advantages of our experimental approach include avoidance of the shadowing error of the pyranometer method and uncertainties related to variability in atmospheric conditions.

The integrating sphere was configured with the sample port at the bottom, a collimated white-light beam introduced from the top and a fibre-optic cable connected to the spectrometer at the side (Supplementary Fig. S5). To avoid the substitution error associated with a single-beam integrating sphere[29], we use the comparison method, wherein the average reflectance and throughput of the sphere remain unchanged when the reflectance standard and snow sample are measured by the spectrometer. This and several additional steps taken to minimize measurement error are described in greater detail in Supplementary Section S5.

The spectrally weighted albedo of snow over the full solar spectrum, α, was calculated from spectrally resolved snow albedo, $\alpha(\lambda)$, and solar spectral irradiance, $i(\lambda)$ with a 5-nm resolution ($d\lambda$) (ref. 28):

$$\alpha = \frac{\int_{300\,nm}^{2,500\,nm} \alpha(\lambda) i(\lambda) d\lambda}{\int_{300\,nm}^{2,500\,nm} i(\lambda) d\lambda} \quad (1)$$

More than ~99% of the surface solar flux is contained in the spectral region between 300 and 2,500 nm. Although our measurements cover the visible and part of the near infrared (395–950 nm) where the BC perturbation is greatest, 36% of the sun's energy lies outside this region[28]. To compute snow albedo over the entire solar spectrum, we considered three spectral regions separately. In the ultraviolet (300–395 nm), we set $\alpha(\lambda)$ equal to the measured α (395 nm). Snow albedo varies little in the ultraviolet[1,14,15]. In the visible and near infrared (395–950 nm) we used the values of $\alpha(\lambda)$ measured in our experiments. In the

infrared (950–2,500 nm), where snow is strongly absorbing and BC has almost no effect on its albedo[1,8,14], we set $\alpha(\lambda)$ equal to the value predicted by SNICAR for pure snow at each R_{eff}.

Received 21 November 2011; accepted 1 February 2012; published online 4 March 2012

References

1. Flanner, M. G., Zender, C. S., Randerson, J. T. & Rasch, P. J. Present-day climate forcing and response from black carbon in snow. *J. Geophys. Res.* **112,** D11202 (2007).
2. Hansen, J. & Nazarenko, L. Soot climate forcing via snow and ice albedos. *Proc. Natl Acad. Sci. USA* **101,** 423–428 (2004).
3. Clarke, A. D. & Noone, K. J. Soot in the arctic snowpack—a cause for perturbations in radiative-transfer. *Atmos. Environ.* **19,** 2045–2053 (1985).
4. Doherty, S. J., Warren, S. G., Grenfell, T. C., Clarke, A. D. & Brandt, R. E. Light-absorbing impurities in Arctic snow. *Atmos. Chem. Phys.* **10,** 11647–11680 (2010).
5. Collins, W. D. *et al.* The formulation and atmospheric simulation of the Community Atmosphere Model version 3 (CAM3). *J. Clim.* **19,** 2144–2161 (2006).
6. Quinn, P. K. *et al.* Short-lived pollutants in the Arctic: Their climate impact and possible mitigation strategies. *Atmos. Chem. Phys.* **8,** 1723–1735 (2008).
7. Grenfell, T. C., Light, B. & Sturm, M. Spatial distribution and radiative effects of soot in the snow and sea ice during the SHEBA experiment. *J. Geophys. Res.* **107,** D8032 (2002).
8. Warren, S. G. & Wiscombe, W. J. A model for the spectral albedo of snow. 2. Snow containing atmospheric aerosols. *J. Atmos. Sci.* **37,** 2734–2745 (1980).
9. Chylek, P., Ramaswamy, V. & Srivastava, V. Graphitic carbon content of aerosols, clouds and snow, and its climatic implications. *Sci. Total Environ.* **36,** 117–120 (1984).
10. Colbeck, S. C. An overview of seasonal snow metamorphism. *Rev. Geophys.* **20,** 45–61 (1982).
11. Flanner, M. G. & Zender, C. S. Linking snowpack microphysics and albedo evolution. *J. Geophys. Res.* **111,** D12208 (2006).
12. Qu, X. & Hall, A. What controls the strength of snow-albedo feedback? *J Clim.* **20,** 3971–3981 (2007).
13. Brandt, R. E., Warren, S. G. & Clarke, A. D. A controlled snowmaking experiment testing the relation between black-carbon content and reduction of snow albedo. *J. Geophys. Res.* **116,** D08109 (2011).
14. Jacobson, M. Z. Climate response of fossil fuel and biofuel soot, accounting for soot's feedback to snow and sea ice albedo and emissivity. *J. Geophys. Res.* **109,** D21201 (2004).
15. Grenfell, T. C., Warren, S. G. & Mullen, P. C. Reflection of solar-radiation by the antarctic snow surface at ultraviolet, visible, and near-infrared wavelengths. *J. Geophys. Res.* **99,** 18669–18684 (1994).
16. Wiscombe, W. J. & Warren, S. G. A model for the spectral albedo of snow. 1. Pure snow. *J. Atmos. Sci.* **37,** 2712–2733 (1980).
17. Conway, H., Gades, A. & Raymond, C. F. Albedo of dirty snow during conditions of melt. *Wat. Resour. Res.* **32,** 1713–1718 (1996).
18. Chylek, P. *et al.* Aerosol and graphitic carbon content of snow. *J. Geophys. Res.* **92,** 9801–9809 (1987).
19. Hadley, O. L., Corrigan, C. E., Kirchstetter, T. W., Cliff, S. S. & Ramanathan, V. Measured black carbon deposition on the Sierra Nevada snow pack and implication for snow pack retreat. *Atmos. Chem. Phys.* **10,** 7505–7513 (2010).
20. Bohren, C. F. Applicability of effective-medium theories to problems of scattering and absorption by nonhomogeneous atmospheric particles. *J. Atmos. Sci.* **43,** 468–475 (1986).
21. Bond, T. C. & Bergstrom, R.W. Light absorption by carbonaceous particles: An investigative review. *Aerosol Sci. Technol.* **40,** 27–67 (2006).
22. Moffet, R. C. & Prather, K. A. *In-situ* measurements of the mixing state and optical properties of soot with implications for radiative forcing estimates. *Proc. Natl Acad. Sci. USA* **106,** 11872–11877 (2009).
23. Warren, S. G. & Wiscombe, W. J. Dirty snow after nuclear-war. *Nature* **313,** 467–470 (1985).
24. Aoki, T. *et al.* Effects of snow physical parameters on spectral albedo and bidirectional reflectance of snow surface. *J. Geophys. Res.* **105,** 10219–10236 (2000).
25. Kirchstetter, T. W. & Novakov, T. Controlled generation of black carbon particles from a diffusion flame and applications in evaluating black carbon measurement methods. *Atmos. Environ.* **41,** 1874–1888 (2007).
26. Chughtai, A. R., Brooks, M. E. & Smith, D. M. Hydration of black carbon. *J. Geophys. Res.* **101,** 19505–19514 (1996).
27. Zuberi, B., Johnson, K. S., Aleks, G. K., Molina, L. T. & Laskin, A. Hydrophilic properties of aged soot. *Geophys. Res. Lett.* **32,** L01807 (2005).
28. Levinson, R., Akbari, H. & Berdahl, P. Measuring solar reflectance-Part II: Review of practical methods. *Sol. Energ.* **84,** 1745–1759 (2010).
29. Gallet, J. C., Domine, F., Zender, C. S. & Picard, G. Measurement of the specific surface area of snow using infrared reflectance in an integrating sphere at 1310 and 1550 nm. *Cryosphere* **3,** 167–182 (2009).

Acknowledgements

This research was financially supported by the Public Interest Energy Research programme of the California Energy Commission and the Atmospheric Systems Research programme of the Department of Energy, Office of Biological and Environmental Research. O.L.H. received financial support from the E.O. Lawrence Fellowship at Lawrence Berkeley National Laboratory. We thank M. Flanner for providing an executable version of the SNICAR model online and modifying it to accommodate our analysis, C. Preble for assistance in our laboratory and T. Novakov for more than a decade of encouragement.

Author contributions

O.L.H. conducted the experiments, ran the model simulations and analysed the data with guidance from T.W.K. O.L.H. and T.W.K. designed the experiments and co-wrote the manuscript.

Additional information

The authors declare no competing financial interests. Supplementary information accompanies this paper on www.nature.com/natureclimatechange. Reprints and permissions information is available online at www.nature.com/reprints. Correspondence and requests for materials should be addressed to O.L.H.

nature climate change

SUPPLEMENTARY INFORMATION

DOI: 10.1038/NCLIMATE1433

Black-carbon reduction of snow albedo

OL Hadley & TW Kirchstetter

Table of Contents

Section 1: Aqueous suspensions of black carbon (BC)

The BC used to contaminate laboratory snow was generated with an inverted diffusion flame of methane and air[1] and collected onto Teflon membrane filters. Figure S1 shows the size distribution of the BC in air. BC laden filters were exposed to ozone at levels in excess of 100 ppm for 20 minutes, which transformed the BC from hydrophobic to hydrophilic[2,3]. Following ozone exposure, each filter was weighed using a microbalance (Sartorius SE2-S). After weighing, the BC was rinsed with pure water from the filter into a volumetric flask. The filters were dried and re-weighed to determine the mass of BC removed. A range of precisely determined concentrations of stably suspended BC in water was used to calibrate the absorbance spectroscopy method discussed below and to make BC contaminated snow (as described in the manuscript).

Section 2: BC concentration in melted snow

BC concentration in snow samples was determined by measuring the absorbance of melted samples using a spectrometer equipped with a liquid waveguide capillary cell (LWCC). The LWCC is a meter long capillary tube coated to prevent scattered light from escaping. The LWCC replaces the cuvette typically used for absorption spectroscopy. Following the Beer-Lambert law, absorbance (A) varied in proportion to the BC concentration of prepared aqueous suspensions:

$$A = \sigma C L \qquad (1)$$

where $A = \ln(I_o/I)$, I_o and I are the intensities of light transmitted through the LWCC containing pure water and an aqueous suspension of BC, respectively, C is the BC concentration (ppm = g m^{-3}), L is the length of the LWCC (1 meter), and σ is a

proportionality constant (m^2 g^{-1}) obtained from the slope of the calibration curve (Figure S2).

Section 3: Mass absorption cross-section (MAC) of BC in air

To determine the MAC of the BC used to contaminate snow (15 ± 1 m^2 g^{-1} at 532 nm), we divided the absorption coefficient (m^{-1}) by the mass concentration (g m^{-3}) of the steady effluent of BC from the diffusion flame. Absorption coefficient was measured using a photo-acoustic instrument[4] and BC mass concentration was determined from the BC mass collected on quartz filters and measured using a thermal-optical analysis method[5].

Section 4: Snow Grain Shape and Effective Radius

Imaging laboratory snow at a magnification of 500x with a digital microscope (Dino-Lite Pro, model AM413TS), we observed that snow grains were spherical (Figure S3). Snow grain size was controlled by varying the pressures applied to the different spray nozzles used when making snow. Effective radius (R_{eff}) was determined from the spectral albedo of snow in the near-infrared. In this spectral region, the albedo of snow is very sensitive to and commonly used to determine effective radius[6-9] We measured the albedo of our snow in the wavelength range from 1000 to 2500 nm using a dual-beam spectrometer (Perkin Elmer Lambda900) equipped with a 15 cm Spectralon integrating sphere, and then we found the effective radii (55, 65, and 110 μm) for which the Snow Ice and Aerosol Radiation (SNICAR) model best simulated the measured spectra (Figure S4). The SNICAR model[10,11], which is described in SI-Section 7, was run with parameters that matched those of our albedo measurements: a solar zenith angle of 0°, a snow density of 550 kg m^{-3}, and direct light in clear sky conditions. We note that the

simulated spectral albedos of infinitely deep snow and snow with a depth of 1 cm are equivalent. This illustrates that our snow samples (5 cm deep, 5 cm in diameter) were sufficiently deep to prevent the infrared radiation from reaching the sample holder surface and biasing our measurements.

Section 5: Minimizing error in snow albedo measured using an integrating sphere-equipped spectrometer

We used an Ocean Optics USB2000+ single beam spectrometer equipped with a 15 cm diameter, integrating sphere (Sphere Optics SPH-6Z-4) to measure snow albedo. The integrating sphere is coated with Zenith UltraWhite, a highly Lambertian material with >98% reflectance from 300 to 2000 nm and an average reflectance of >95% over the solar spectrum. The reflectance standard (Sphere Optics, model SG 3088 Zenith Reflectance Standard 99%) we used is made of the same material and came supplied with calibration data specifying the true reflectance of the standard at each wavelength between (250 – 2500 nm), traceable to NIST standards. The following describes the integrating sphere configuration and steps taken to reduce measurement error.

1) To avoid the substitution error associated with a single beam integrating sphere[12], we used the comparison method to measure snow albedo[13]. The substitution error is inherent in single beam integrating spheres that measure reflectance. It is caused by the difference in the throughput of the sphere when the reference (i.e., the reflectance standard) makes up a portion of the sphere wall and when a sample of different reflectance is substituted for the reference. In the comparison method, one spectrometer scan is recorded when the reference is at the sphere's reflectance port and the sample is at a port that is normal to the reflectance port (Figure S5b). The positions of the sample and

reference are swapped and a second scan is recorded (Figure S5a). Therefore, the average reflectance and throughput of the sphere remain unchanged from the reference to the sample scan.

2) One potential source of bias in our snow albedo measurements the emergence of reflected radiation to the exterior surface of the sphere rather than into the sphere's reflectance port. Another is the absorption of radiation that reaches the snow sample holder. To minimize the loss of light to the exterior of the integrating sphere and to the snow sample holder, the area of the collimated light incident on snow samples (0.27 cm^2) was kept small compared to the area of the reflectance port (11.45 cm^2) and sample holder (20.3 cm^2). Also, snow samples were densely packed to maximize the optical depth and reduce the distance that radiation traveled in the snow sample holder (see SI-Section 6).

3) A baffle was installed inside the sphere between the sample port and the sphere wall opposite the fiber-optic port to prevent detection of specular components of light reflected from snow samples. While snow reflectance is approximately Lambertian, specular reflectance of wavelengths greater than 700 nm have been reported[6]. Compared to diffusely reflected light from the Lambertian reflectance standard, the intensity of specular components of reflected light from snow would be more intense, and this could potentially bias snow albedo measurement. A baffle between the sample and fiber-optic ports was unnecessary because the narrow viewing angle of the fiber prevented detection of possible specular components of reflected light.

Section 6: Adjusting for light lost to snow sample holder during albedo measurements

Snow was densely packed (550 kg m^{-3} versus a typical value of 200 kg m^{-3} for natural snow) into a sample holder (5 cm deep, 5 cm in diameter) aiming to maximize optical depth and minimize the fraction of radiation incident on the snow's surface that reached and, thus, would be absorbed by the holder (which was black in color). A small fraction of the incident light did, however, penetrate the snow and reach the holder, which biased low the measured snow albedo. To remove the influence of the sample holder, all values of measured snow albedo were multiplied by the wavelength-, snow grain size-, and BC content-specific values shown in Figure S6. The resulting (i.e., adjusted) albedo values reported in this manuscript are, therefore, representative of snow of infinite depth.

The values in Figure S6 are the ratio of the albedo of infinitely deep snow to the albedo of snow with a density of 550 kg m^{-3}, a depth of 2 cm, and an underlying black surface (matching our experimental conditions). The albedo of infinitely and 2 cm deep snow was estimated using the SNICAR model, run with snow grain sizes and BC concentrations that matched those of our experiments. Two centimeters is the depth our snow samples would be if their volume was spread evenly over the surface area of the sample holder.. The largest albedo adjustment (an increase of ~6% in the visible spectral region) corresponded to pure snow with 110 μm R_{eff} (Figure S6). Smaller albedo adjustments were necessary for 65 and 55 μm R_{eff} pure snow (increases of ~3% and 1%, respectively). The albedo of BC contaminated snow samples was generally adjusted by less than 1%, arguably not significant given the uncertainty in our albedo measurements (Figures 1 & 2). These adjustments yield albedos for pure snow that closely agree with those simulated by SNICAR, consistent with previous studies that have verified the

accuracy of radiation transfer models of pure snow. The smaller adjustments needed for snow with smaller grains and for BC contaminated snow are intuitively correct because smaller grains and BC contamination increase optical depth. The very small adjustment needed for BC contaminated snow samples indicates that the optical depth was sufficiently high to prevent a significant fraction of incident light from reaching the sample holder. In all cases, the correction factor was very small in the infrared spectral region where snow is strongly absorbing.

Section 7: Snow Ice and Aerosol Radiation (SNICAR) model

SNICAR calculates snow albedo as the ratio of the upward and downward flux at the snow surface. In this study, SNICAR parameters were set to match our method of albedo measurement: direct sunlight, solar zenith angle of 0°, and clear sky conditions. The surface incident solar flux used by SNICAR was produced with the atmospheric Shortwave Narrowband Model (SWNB)[14,15]. This surface spectrum is identical to the surface solar spectrum[16] we used to calculate the albedos shown in Figure 2. The radiative transfer solution is a single-layer version of the multiple scattering, multi-layer, approximation described by *Toon et al.* (1989)[17], with the delta-hemispheric mean approximation[10]. Snow is treated as a log-normal distribution of ice spheres. Mie parameters are calculated off-line at high spectral resolution for lognormal distributions of ice spheres with effective radii ranging from 30 to 1500 μm[11]. Broadband albedo is weighted by the incident solar flux[11].

SNICAR assumes a log-normal size distribution of BC with a median radius of 0.05 μm and a standard deviation of 1.5. The index of refraction of the BC was taken from Chang and Charalampopoulos [1990][18] and varies with wavelength. At 540 nm, the

specified refractive index of BC is 1.77 - 0.63i. Using the prescribed size distribution, refractive index, and Mie theory, the BC particle mass density is tuned to obtain a spectrally resolved mass absorption cross section (MAC), which has a default value of 7.5 m^2 g^{-1} at 550 nm. Thus for a given BC mass concentration in snow, the model computes the appropriate number concentration with the previously mentioned physical and optical properties. To scale the MAC to larger and smaller values, the mass extinction cross-section (across the spectrum) is multiplied by a constant scalar specified by the user. Since single-scatter albedo remains constant, this operation scales the mass absorption cross-section by the same factor.

Supplementary References:

1. Kirchstetter, T.W. & Novakov, T. Controlled generation of black carbon particles from a diffusion flame and applications in evaluating black carbon measurement methods. *Atmospheric Environment* **41,** 1874-1888 (2007).

2. Akhter, M.S., Chughtai, A.R. & Smith, D.M. Spectroscopic Studies of Oxidized Soots. *Applied Spectroscopy* **45,** 653-665 (1991).

3. Chughtai, A.R., Brooks, M.E. & Smith, D.M. Hydration of black carbon. *Journal of Geophysical Research-Atmospheres* **101,** 19505-19514 (1996).

4. Arnott, W.P. *et al.* Photoacoustic and filter-based ambient aerosol light absorption measurements: Instrument comparisons and the role of relative humidity. *Journal of Geophysical Research-Atmospheres* **108,** 4034, doi:4010.1029/2002JD002165 (2003).

5. Kirchstetter, T.W., Corrigan, C.E. & Novakov, T. Laboratory and field investigation of the adsorption of gaseous organic compounds onto quartz filters. *Atmospheric Environment* **35,** 1663-1671 (2001).

6. Aoki, T. *et al.* Effects of snow physical parameters on spectral albedo and bidirectional reflectance of snow surface. *Journal of Geophysical Research-Atmospheres* **105,** 10219-10236 (2000).

7. Brandt, R.E., Warren, S.G. & Clarke, A.D. A controlled snowmaking experiment testing the relation between black-carbon content and reduction of snow albedo. *Journal of Geophysical Research-Atmospheres* **116**(2011).

8. Wiscombe, W.J. & Warren, S.G. A Model for the Spectral Albedo of Snow .1. Pure Snow. *Journal of the Atmospheric Sciences* **37,** 2712-2733 (1980).

9. Grenfell, T.C., Warren, S.G. & Mullen, P.C. Reflection of Solar-Radiation by the Antarctic Snow Surface at Ultraviolet, Visible, and near-Infrared Wavelengths. *Journal of Geophysical Research-Atmospheres* **99,** 18669-18684 (1994).

10. Flanner, M.G., http://snow.engin.umich.edu/.

11. Flanner, M.G., Zender, C.S., Randerson, J.T. & Rasch, P.J. Present-day climate forcing and response from black carbon in snow. *Journal of Geophysical Research-Atmospheres* **112,** - (2007).

12. Gallet, J.C., Domine, F., Zender, C.S. & Picard, G. Measurement of the specific surface area of snow using infrared reflectance in an integrating sphere at 1310 and 1550 nm. *Cryosphere* **3,** 167-182 (2009).

13. Workman, J. & Springsteen, A.W., *Applied Spectroscopy: a compact reference for practitioners*. (Academic Press, San Diego, CA, 1998).

14. Stamnes, K., Tsay, S.C., Wiscombe, W. & Jayaweera, K. Numerically Stable Algorithm for Discrete-Ordinate-Method Radiative-Transfer in Multiple-Scattering and Emitting Layered Media. *Applied Optics* **27,** 2502-2509 (1988).

15. Zender, C.S. *et al.* Atmospheric absorption during the Atmospheric Radiation Measurement (ARM) Enhanced Shortwave Experiment (ARESE). *Journal of Geophysical Research-Atmospheres* **102,** 29901-29915 (1997).

16. Levinson, R., Akbari, H. & Berdahl, P. Measuring solar reflectance-Part II: Review of practical methods. *Solar Energy* **84,** 1745-1759 (2010).

17. Toon, O.B., Mckay, C.P., Ackerman, T.P. & Santhanam, K. Rapid Calculation of Radiative Heating Rates and Photodissociation Rates in Inhomogeneous Multiple-Scattering Atmospheres. *Journal of Geophysical Research-Atmospheres* **94,** 16287-16301 (1989).

18. Chang, H. & Charalampopoulos, T.T. Determination of the Wavelength Dependence of Refractive-Indexes of Flame Soot. *P Roy Soc Lond a Mat* **430,** 577-591 (1990).

Supplementary Figures

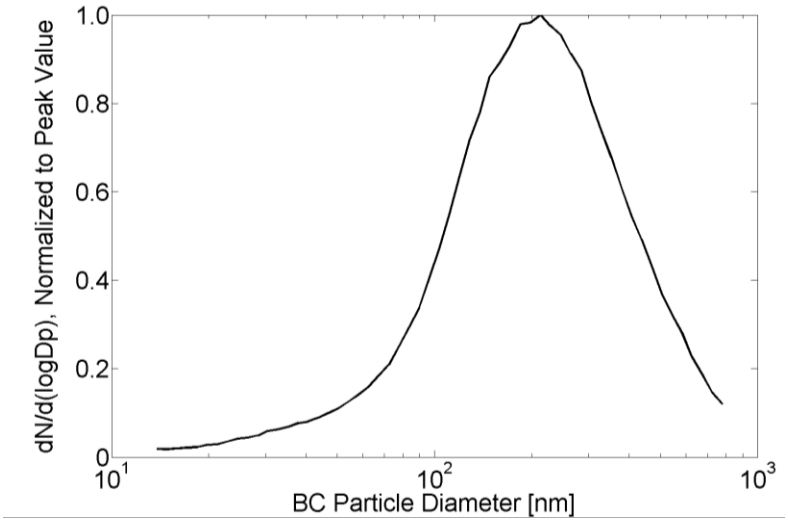

S1. Normalized size distribution of the flame-generated BC in air.

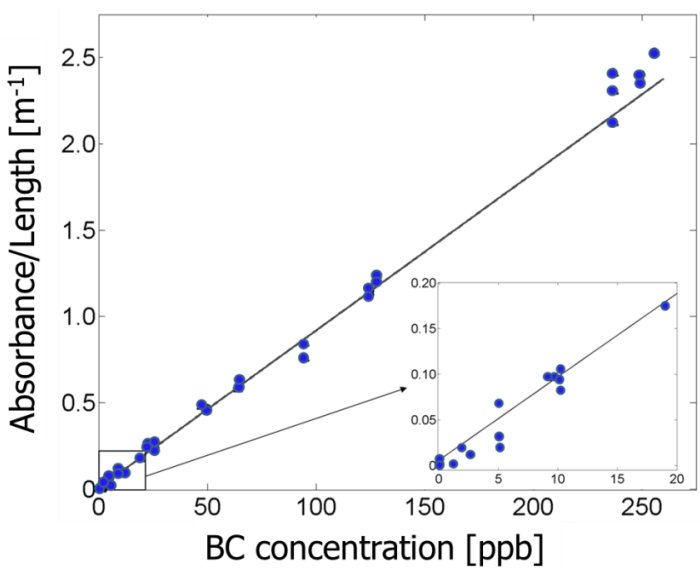

S2. Linear relationship between absorbance and BC concentration in water used to estimate BC concentration in melted laboratory snow samples. Absorbance measurements were made at 550 nm using a spectrometer equipped with a 1 m long liquid waveguide capillary cell (LWCC).

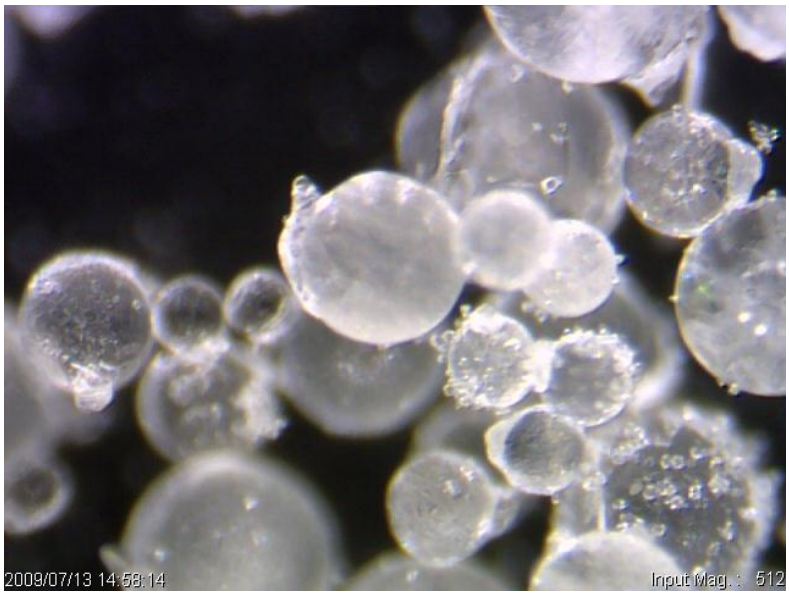

S3. Laboratory snow grains at a magnification of 500x.

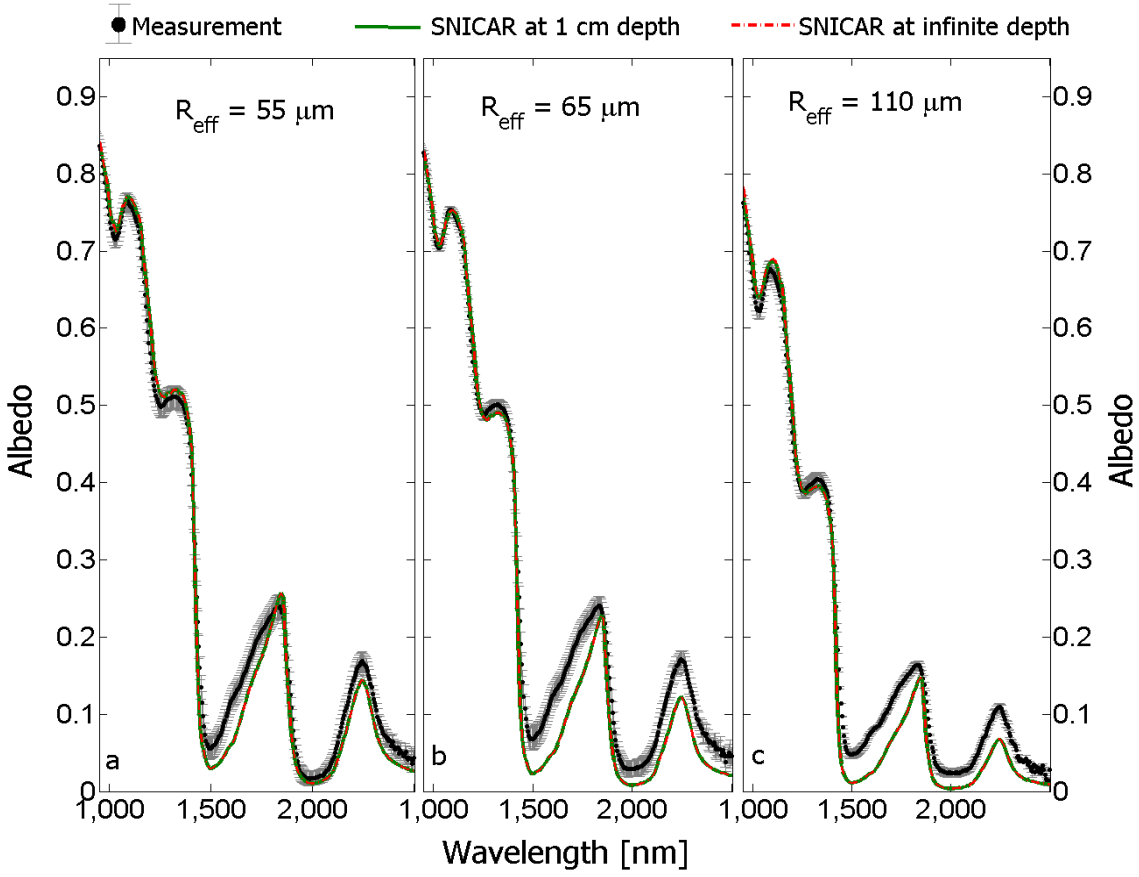

S4. Albedo of snow in the infrared spectral region (950 to 2500 nm) measured in our laboratory and matched by the SNICAR model.

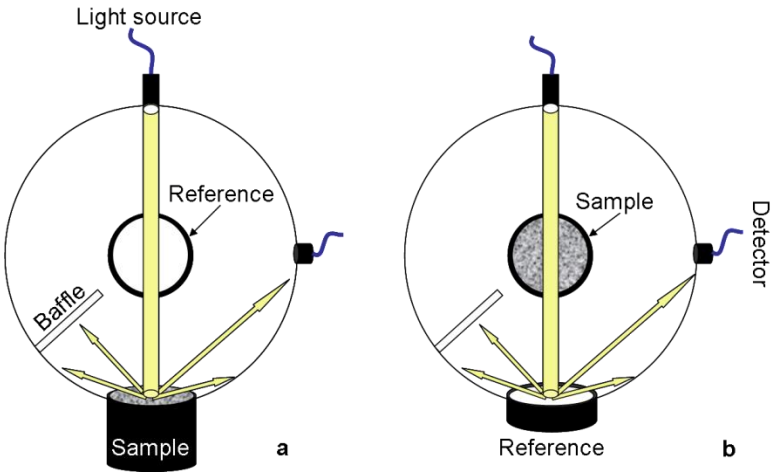

S5. The reflectance of snow samples was measured with a spectrometer equipped with an integrating sphere using the comparison method illustrated here. In this method, both reflectance standard and snow sample are placed at sphere ports when the reflectance of the (a) snow sample and (b) reflectance standard are measured.

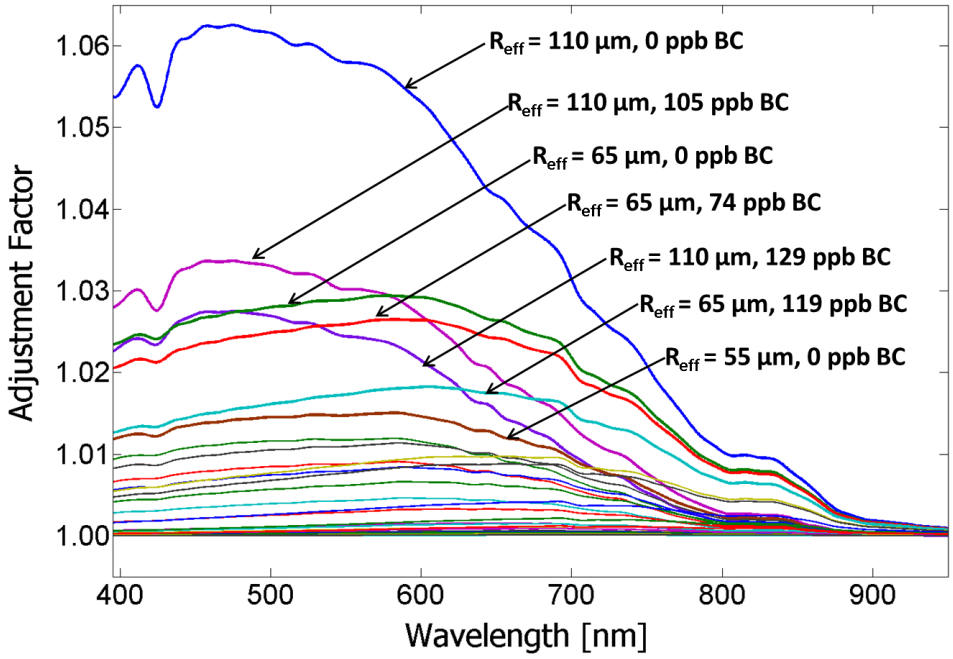

S6. Values of measured snow reflectance were multiplied by these wavelength-, snow grain size-, and BC content-specific values to correct for light lost to the snow sample cup. Values of snow albedo reported in this manuscript are, therefore, representative of snow of infinite depth.